24th COBEM - 2017

24th ABCM International Congress of Mechanical Engineering
December 3-8, 2017, Curitiba, PR, Brazil

COBEM-2017-1593
EXPERIMENTAL STUDY OF LAMINAR NON PREMIXED ETHYLENE/AIR FLAMES USING LASER INDUCED INCANDESCENCE AND FLUORESCENCE

Juan José Cruz Villanueva
Luís Fernando Figueira da Silva
Departamento de Engenharia Mecânica, Pontifícia Universidade Católica do Rio de Janeiro, Rio de Janeiro, Brazil
juancruz@aluno.puc-rio.br - luisfer@ puc-rio.br

Andrés Fuentes Castillo
Departamento de Industrias, Universidad Técnica Federico Santa Maria, Valparaiso, Chile
andres.fuentes@usm.cl

Abstract. *In this work is presented a combined planar laser induced fluorescence (PLIF) and laser induced incandescence (LII) study of laminar premixed ethylene/air flames. These flames are stabilized at a Gülder burner. Both the fluorescence and incandescence processes are excited using a pulsed UV (266nm) laser source. The soot signal corresponding to a delayed signal detection by an intensified camera, whereas the prompt detection should involve the simultaneous soot and polycyclic aromatics hydrocarbons (PAH) presence. The calibration of LII signal to soot volume fractions is achieved by means of line of sight attenuation methodology. Two band-pass filters (*$400\ nm$ *and* $550\ nm$*) have beem used, so as to evidence different regions within the flame. The soot region radiation is used to measure the temperature fields by two-color pyrometry using a pair of filters (*$530\ nm$ *and* $900\ nm$*). The results demonstrate that, at the colder region, near the fuel inlet, PAH seem to prevail. Following this region, in a warmer mid–height zone, both soot and PAH appears to coexist. Near the flame tip soot is found only.*

Keywords: *PAHs, Soot, LII, LIF, Two-color pyrometer.*

1. INTRODUCTION

Exhaust gases from industrial furnaces or diesel engines, for example, may release atmospheric pollutants, including polycyclic aromatic hydrocarbons (PAHs), nitrogen oxides (NOx), unburnt hydrocarbons (HC), Carbon monoxide (CO) and particulate material (PM). PAHs are organic compounds formed by several aromatic rings (Fetzer, 2000) and which are considered to be pollutants with potential carcinogenic and mutagenic effects on living organisms (Luch, 2005). Soot represents commonly an agglomerate of carbonaceous primary particles, whose dimensions lie between $5 - 30\ nm$ (Bladh, *et al*., 2009; Bladh, *et al*., 2011; De Luliis, *et al.*, 2011), formed in the combustion process as a result of incomplete hydrocarbon burning. These particles are harmful to the human health but, in certain industrial applications, their presence is favorable to increasing the radiation release by the flame. In combustion processes, PAHs lie in the thermochemical pathway between the smaller fuel fragments, acetylene, for instance, and the formation of soot particles (Frenklach, 2002), being precursors of these. In this context, it is important to understand the PAHs and soot formation and consumption processes, their distribution along the flame and the ways of promoting their oxidation. This can be effected by several methods, such as: the collection of the material and its gravimetric measurement; absorption spectroscopy, in which the absorption of light radiation by the soot is measured; laser induced incandescence, among others (Schulz, *et al.*, 2006; Desgroux, *et al.*, 2013).

Laser diagnostic techniques may spatially locate and characterize the PAHs, via laser induced fluorescence (LIF) (Desgroux, *et al.*, 2013), and soot, via laser induced incandescence (LII) (Schulz, *et al.*, 2006). This may be achieved using UV-Visible or UV-IR laser excitation wavelengths respectively. The comparison of the LII signal (at the IR range) with simultaneously LII+LIF, at the UV range, allows to qualitatively discriminate the PAHs and soot regions. In ethylene/air non-premixed coflow flames, the PAHs are found to occur in the inner region, near the burner exit. In such flames, PAHs are surrounded by the soot region, separated by a thin dark region where soot precursors transformation into solid carbonaceous soot occurs (Vander Wal, 1996; Vander Wal, 1998). Based on the fluorescence peaks shifts to

the infrared (IR) range with the PAHs size increase (Bejaoui, *et al.*, 2014), PAHs distribution along the flame has been studied using different spectral detection bands (Vander Wal, *et al.*, 1997). The PAH/Soot separation region is found to be present in low sooting flames, such as methane diluted, but could disappear leading to soot and PAH co-existing in a relative large region when the dilution is increased (Schoemaecker Moreau, *et al.*, 2004). The PAHs fluorescence signal, which lifetime is of the order of tens of nanoseconds, rapidly decreases, when compared with that soot of incandescence, which lifetimes is the order of hundreds of nanoseconds. As consequence, a variable window camera detection (prompt-delay) approach allows to discriminate PAH and Soot by using a single UV-Visible laser excitation (Vander Wal, *et al.*, 1997; Bouvier, *et al.*, 2007). In order to observe the LII region only, the delayed signal (LII) is considered. The PAHs distribution is found to be the result of prompt (LIF+LII) signal subtracted by minus the delayed signal (Bouvier, *et al.*, 2007).

Laminar coflow non premixed flames are axially symmetric 2-D flames with good stability properties. These flames classically provide means to study combustion phenomena and are currently used as target flame to LII calibration (Schulz, *et al.*, 2006). The Gulder burner (Snelling, *et al.*, 1999) stabilizes strongly sooting flames that have been use as means of allowing soot characterization (Schulz, *et al.*, 2006). However, to the best of our knowledge, little studies have been conducted on the soot precursors growth in such flames. Therefore, with the objective of improving the understanding precursor grow and soot production, non-premixed ethylene/air flames are studying in this work. This study is performed using UV excitation and variable spectral detection with different band-pass filters. Additionaly, temperature fields in the soot region is measured using two-color pyrometry (Escudero, *et al.*, 2016a).

2. METHODOLOGY

In the following section, the burner configuration and case of studied are presented. In addition, each experimental setup and procedure to obtain PAHs formation, soot distribution and soot temperature is described.

2.1 Burner and experimental conditions

The experiments are performed using a Gülder burner with dimensions identical to those given by (Snelling, *et al.*, 1999), which is commonly used to study the soot formation in a laminar and axisymmetrical non-premixed flames (Snelling, *et al.*, 2002; Hadef, *et al.*, 2013). The burner structure with ethylene flame, shown in Fig. 1, is composed of a 11 mm internal diameter central fuel injection tube, made of stainless steel, and an external concentric tube with 100 mm diameter that forms an annular air flow duct. The burner cross section evidences the base air inlets, which consist of through four ¼" NPT connections. Downstream to these inlets two porous discs create a settling chamber which is filled with 6 mm spheres, intended to remove vorticity of the air flow, thus allowing for stable flames to occur (Borshanpour and Bobby, 2013). Two mass flow meters are used, Alicat Scientific MC-500SCCM-D/5M and MCH-100SLPM-D/5M, for ethylene and air flows, respectively, with a 0.8 % maximum reading uncertainty for the fuel injection and 0.2% for the oxidizer.

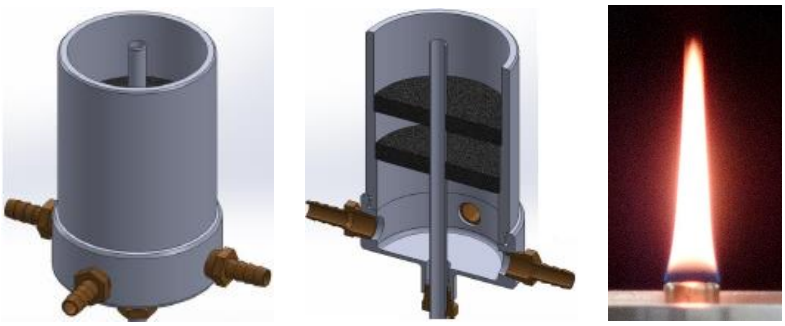

Figure 1. (a) Gülder burner and (b) Ethylene flame.

The operating conditions established for the calibration flame in the Gülder burner, also known as "Gülder flame", are $V_f = 0.194\ slpm$ $(3.23\ cm^3/s)$ for ethylene, and $V_{air} = 284\ slpm$ $(4{,}733\ cm^3/s)$ for air (at $21°\ C$ and $1\ bar$) (Schulz, *et al.*, 2006). This leads to a stable laminar flame of height $h_f \approx 65$ mm in height, obtained near the smoke point, i.e., the condition at which soot escapes from the flame tip (Gülder, *et al.*, 1996; Schulz, *et al.*, 2006). For this calibration condition, a stable flame has been observed in two color pyrometry measurements. However, flickering near the flame tip has been is evidenced in the laser induced measurements and LIF and LII results not are analyzed for this particular case.

Table 1 shows the different combustion cases studied in this work, where the fuel flow rate varied from $V_f = 0.08\ slpm$ ($1.33\ cm^3/s$) to $0.194\ slpm$ and the air flow rate is always $V_{ar} = 60\ slpm$ ($1{,}000\ cm^3/s$). The air flow rate is limited by the available steady state pressure that can be attained in the compressed air feed line. This is the reason why the used flow rate is smaller than the classical Gülder one. However, even if the oxidizer flow rate is four times smaller than that of the Gülder experiment, the flame is still sufficient hyperventilated for the purposes of this study. The flame height, h_f, reported in Tab. 1, is the maximum vertical coordinate where the flame emission image at $431 \pm 5\ nm$ is observed. The fuel flow mass rate, m_f, is calculated using a density of $\rho_f = 1.167\ \mathrm{kg/m^3}$, at $T = 20°\ C$. An estimate of the residence time, τ_{res}, defined as h_f/u_f, where, u_f, is the bulk velocity, is also given in Tab. 1.

Table 1. Combustion cases of study to ethylene and air flame. $\dot{V}_{ar} = 60\ slpm$.

Case	$\dot{V}_{C_2H_4}$ $[sccm]$	h_f $[mm]$	$\dot{m}_f$ $\left[\frac{kg}{s}.10^{-6}\right]$	u_f $\left[\frac{mm}{s}\right]$	τ_{res} $[s]$
A	80 ± 1.6	23.9	1.56	14.0	1.70
B	100 ± 1.8	31.6	1.95	17.5	1.80
C	121 ± 2.0	39.7	2.35	21.2	1.87

2.2 LIF and LII techniques measurements

Figure 2(a) shows the setup for the simultaneous excitation of PLIF and LII signals. Excitation is performed with the 4th harmonic ($266\ nm$) of a *Brilliant b* (Quantel) Nd: YAG laser (Cignoli, *et al.*, 1992; Vander Wal, 1996; Vander Wal, *et al.*, 1997; Vander Wal, 1998), with $80\ mJ$ nominal energy, and operated at $10\ Hz$. A dichroic mirror filters the second harmonic ($532\ nm$) residual component. An energy monitor (LaVision) is used to sense pulse energy variation, in order to reject results produced by laser energy fluctuations larger than a standard deviation. The laser beam is transformed into a thin planar sheet of $0.25 \times 25\ mm$, which passes through the center of the flame, using two pairs of lenses. The first two spherical lenses, $f = -80\ mm$ and $100\ mm$, converge the beam to the desired thickness and the second pair of cylindrical lenses, $f = -50\ mm$ and $150\ mm$, vertically expands the beam. The laser fluence curve measure for this flame indicate which the *plateau* region, i.e. region where LII signal is independent of laser fluence, is founded above $0{,}08\ J/cm^2$. For this reason, this value is used in this work.

The images are captured by means of an intensified model *IRO* (*Intensified relay optics*) LaVision with a P43 photosensor, coupled to an *Imager Intense* CCD camera (LaVision) with 1376×1040 pixel resolution, arranged perpendicular to laser sheet. The measured spatial resolution is approximately $26\ px/mm$ DAVIS 8.1 software is used to control the trigger signal of lasers and cameras. A lens Nikon Rayfact PF10545MF-UV and different interference filters centered at the wavelengths of 400 and $550 \pm 12.5\ nm$ with 90% of transmissivity are used in order to perform PAH's and soot spectral characterization, following previous studies (Xiao, *et al.*, 2005). Delayed detection with respect to laser pulse, $> 50\ ns$, avoids the PAHs fluorescence signal and is supposed to represent soot incandescence only. Thus, a single camera gate of $20\ ns$ and two distinct initial detection times $0\ ns$ (prompt) and $50\ ns$ (delay) are used to distinguish between LIF and LII signal. One hundred of single shot images are used to obtain the average field for each case.

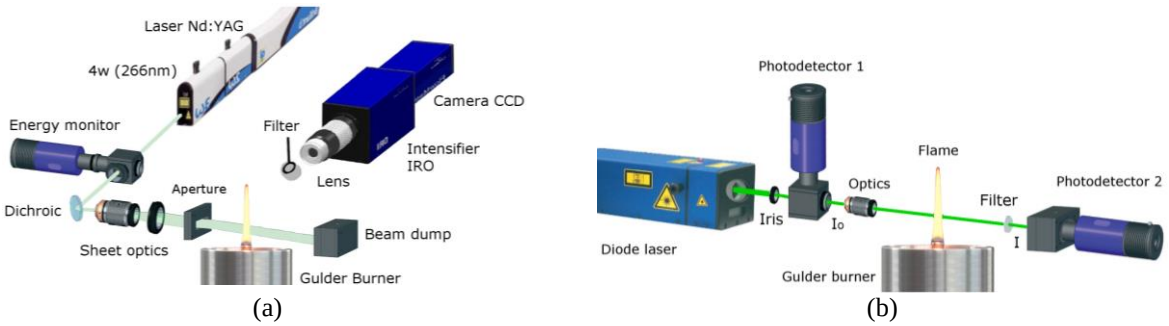

Figure 2. (a) Sooting flame at Gulder burner, (b) Experimental setup of simultaneous $\boldsymbol{LIF + LII}$ and light extinction.

In order to obtain soot volumetric fraction values, the LII results calibration is performed by laser extinction measurements, as shown in Fig. 2(b). A continuous diode laser beam at $532\ nm$, model *DPSS-0,5W-CW* (LaVision), is

used with two energy monitors LaVision, located before and after the flame. An iris is used to select a $4\,mm$ diameter beam central region with $35.5\,mW$ also measured with Gentec Solo $UP19K-15S$. With the aim of obtaining a $330\,\mu m$ spatial resolution, the first pair of lenses described in the previous paragraph is used. The flame luminosity is rejected by a line laser filter ($532\,nm$) located in front of the second energy monitor. Classically, the measured energy transmissivity is related to path mean soot volume fraction $\overline{f_v}(y_0)$ (Zhao and Ladommatos, 1998). Thus, the soot volume fraction of the LII image is obtained as $f_v(x,y) = C_{cal} \cdot S_{LII}(x,y)$, where $C_{cal} = \overline{f_v}(y_0)/\bar{S}_{LII}(x,y)$.

2.3 Two color pyrometry meaurements and determination of temperature radial profiles

The two color pyrometry technique is based on the measured flame natural soot radiative emission at two different wavelengths. In this work, this measurement is performed using direct capture by an *Imager Intense* LaVision CCD camera only, since the signal intensity is strong enough. The CCD camera exposure time is $800\,\mu s$ and $24\,px/mm$ resolution is used, with two interference filters centered at wavelengths of $530 \pm 5\,nm$ and $900 \pm 5\,nm$ and with ~ 53 % of transmissivity. In this case, 100 images are taken for each wavelength.

Since the single camera images represent line-of-sight flame emission measurements, it is necessary to perform a mathematical treatment so as obtain the radial fields along the flame centerline. The solution of the radiative transfer equation associated to the soot radiation results in an integral Abel equation, that is discretized following (Liu and Jiang, 2001). This equation requires the knowledge of soot extinction coefficient. However, flames similar to those studied here have been shown to be optically thin (Snelling, *et al.*, 2002; Liu, *et al.*, 2013). Such a hypothesis has been addressed (Jenkins and Hanson, 2001; Henríquez, *et al.*, 2014; Legros, *et al.*, 2015; Escudero, *et al.*, 2016a; Escudero, *et al.*, 2016b) and, thus, the self-absorption of soot is not considered here. The discretized radiative transfer equation is solved by an onion peeling algorithm (Dasch, 1992) with zero-order Tikhonov regularization (Daun, *et al.*, 2006), which allows for the radial intensity distribution to be obtained. The Planck function, modified by soot emissivity, models the flame soot emission (Modest, 2013). Therefore, the local temperature may be obtained from the intensity ratio at two wavelengths (Jenkins and Hanson, 2001; Escudero, *et al.*, 2016a), without the need to use a calibration factor.

3. RESULTS AND DISCUSSION

3.1 Soot and PAH's distributions

Figure 3 shows images of the prompt (left side) and delay (right side) excited signals corresponding to case B, captured with $400\,nm$ and $550\,nm$ interference filters. The corresponding radial profiles of LIF and LII at three dimensionless height, $z/h_f = 0.2, 0.4, 0.6$, are shown in Fig. 4 for the two wavelengths. In this figure, the profiles are normalized with respect to the maximum value at each height and detection filter. Comparing, first, the delayed detection results, one may observe a nearly identical intensity distribution, which indicates that only soot is responsible for the measured signal at both wavelengths and for $t > 50\,ns$. At $z/h_f = 0.2$, soot is found to exhibit a maximum value for $r \approx 3.5\,mm$ and is nearly absent at the centerline. Further downstream, at $z/h_f = 0.6$, the maximum value position moves closer to the centerline ($r \approx 2\,mm$) and significant amounts exist at $r \approx 0$. Closer to the flame tip ($z/h_f = 0.8$), soot distribution is monotonical with r, and the maximum occurs at the centerline. This soot distribution pattern is classical and has been observed for flames lying below the smoke point, such as the studied by (Henríquez, *et al.*, 2014).

Figure 4 allows to verify that the prompt and delayed signals at both wavelengths are also nearly identical for $z/h_f = 0.8$, but differ significantly at the lower parts of the flame. This is an indicator that only soot remains at this larger flame height. However, at lower regions of the flame and close to the centerline, the normalized $550\,nm$ prompt signal is smaller that the prompt value measured at $400\,nm$. Significant signal decay at these regions occurs: for instance, at $z/h_f = 0.6$, the centerline prompt signal is ≈ 0.8, whereas the delayed one is ≈ 0.6. Such a difference could be indicative of the PAH presence. At this height, the difference between 550 nm and 400 nm measured values lie within the experimental uncertainty bounds. There, it seems impossible to assign these signals to PAHs of different molecular weights.

The most important difference observed between the filters and the delays is found at $z/h_f = 0.2$. Indeed, the radial distribution of these measurements suggest that the species responsible for the prompt signal have maximum values that lie at different radial positions. Concerning now the prompt and delayed signals, these evidence that, at $550\,nm$, only minor differences are observed at $r \approx 0$. Therefore, detection at $400\,nm$ should allow to identify the respective location of the smaller PAHs and soot regions, which are found to qualitatively agree with that of previous works (Vander Wal, 1996; Vander Wal, *et al.*, 1997).

The effect of the fuel flow rate on the measured $400\,nm$ signals is evidenced in Fig. 5 at three dimensionless height, $z/h_f = 0.2, 0.4, 0.6$. For these three flow rates and heights, a maximum value is always observed and corresponds to the presence of soot as evidenced by the delayed signals, not shown here for the sake of brevity. Following the discussion above, it may be assumed that the centerline ($r \approx 0$) measurement represent PAHs at the lower part of the flame, and a combined effect of soot and PAHs at $z/h_f = 0.6$. Thus, for $z/h_f = 0.2$, increasing the fuel flow leads to a decrease of

the prompt signal. This prompt signal is also found to exhibit a local maximum, which should correspond to the PAH production.

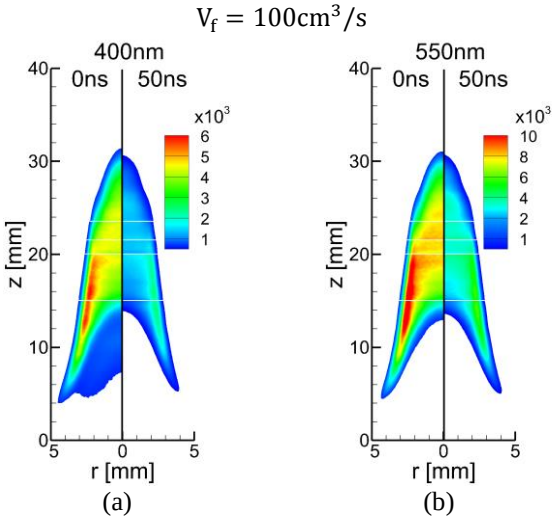

Figure 3. Average fields of LIF and LII signal of Case B to (a) $\mathbf{400}\ \boldsymbol{nm}$ e (b) $\mathbf{550}\ \boldsymbol{nm}$. Prompt detection $\mathbf{0}\ \boldsymbol{ns}$ (left) and delay detection $\mathbf{50}\ \boldsymbol{ns}$ (right).

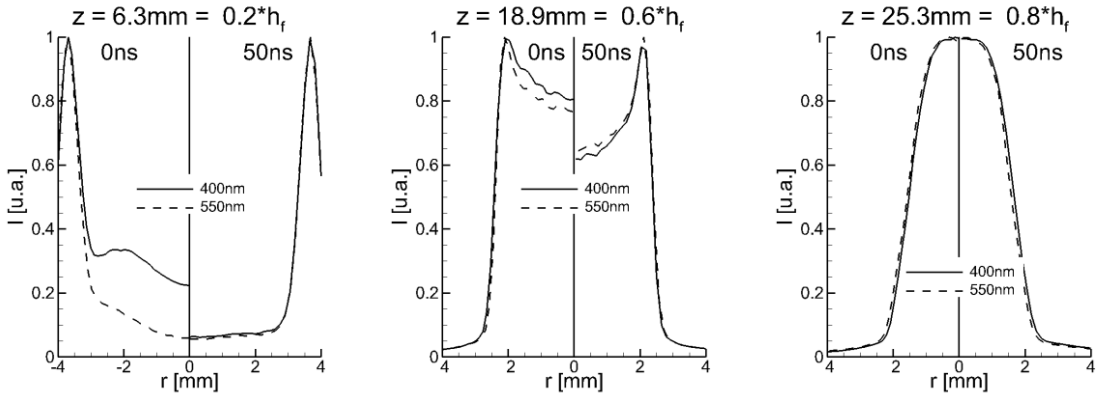

Figure 4. Radial profiles of LIF + LII signal of Case B at (a) $\boldsymbol{z/h_f = 0.4}$, (b) $\boldsymbol{z/h_f = 0.6}$ e (c) $\boldsymbol{z/h_f = 0.8}$.

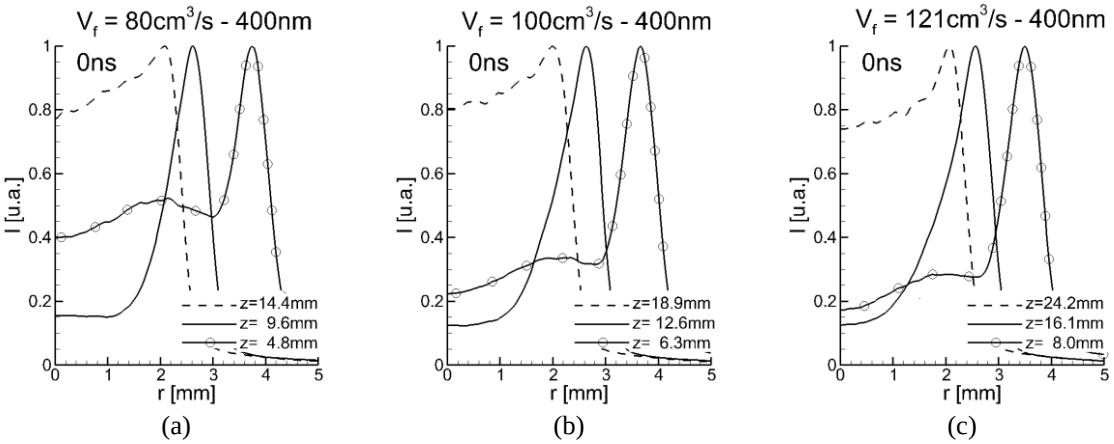

Figure 5. Radial profiles of the prompt signals at $\boldsymbol{z/h_f = 0.2}$, $\mathbf{0.4}$ e $\mathbf{0.6}$, to (a) Case **A**, (b) Case **B**, (b) Case **C**.

3.2 Soot pyrometry field

The soot temperature fields deduced from 530 nm (visible) and 900 nm (infrared) local emission rate are show in Fig. 6 for case A, B e C. The corresponding radial profiles at different heights are given in this Fig. 7. Comparing Fig. 6 with Fig. 3, it should be evident, as expected, that temperature can only be computed where soot is present. This is the reason why high temperature values seem to be located at the "oxider side" and, also, that unrealistic temperature values at the fuel tube region need to be discarded. Fig. 6 and Fig. 7 indicate that, for the three examined flow rates, the maximum temperature at the lower part of the flame ($z/h_f = 0.4$) is nearly invariant, whereas the centerline temperature significantly increases (from 1500 K to 1600 K) with the fuel flow rate. On the other hand, closer to the flame tip ($z/h_f = 0.8$), the radial temperature distribution is nearly constant and decreases (from 2100 K to 1900 K) when the fuel flow rate increase. The depicted intermediate height ($z/h_f = 0.4$) behavior is somewhat characteristic of the tip region, since the overall temperature values decrease, albeit exhibiting a significant difference between the centerline and the maximum temperatures region.

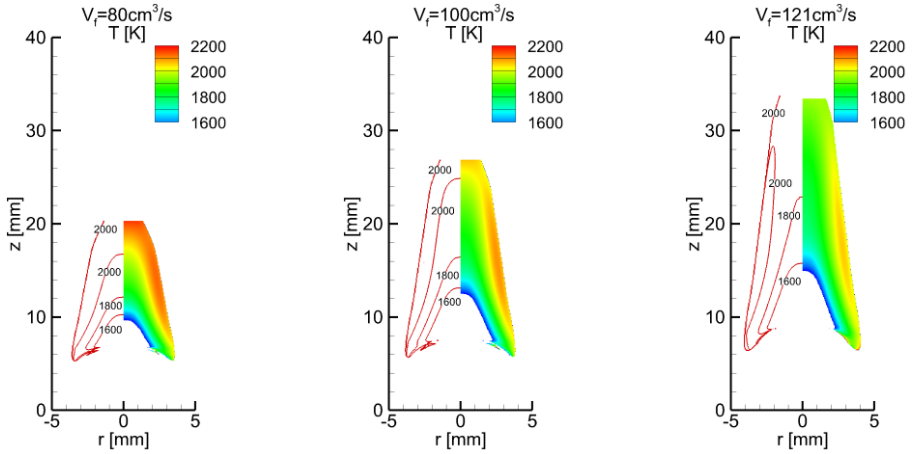

Figure 6. Temperature fields and iso-contour of (a) Case A, (b) Case B, (b) Case C.

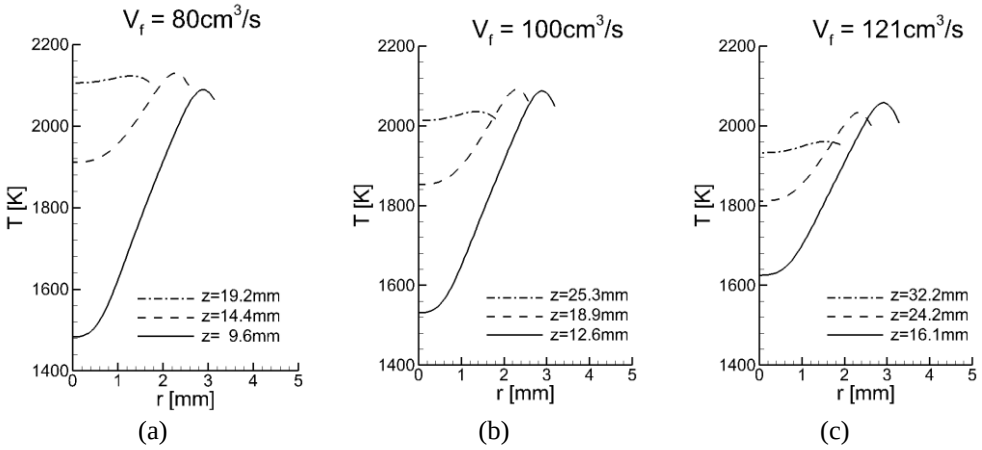

Figure 7. Radial profiles temperatures at $z/h_f = 0.4$, 0.6 e 0.8, to (a) Case A, (b) Case B, (b) Case C.

4. CONCLUSIONS AND PERSPECTIVES

This work has presented the first results obtained of the characterization of temperature, soot and PAH in laminar non premixed flames of ethylene and air. This characterization was performed using two color pyrometry, laser induced incandescence and laser induced fluorescence. The obtained results allow to distinguish three regions within the flames: (1) a high temperature region where soot is found, (2) an intermediate temperature region, where PAH and soot seem coexist and (3) a lower temperature region, where the prompt (LIF) signal indicates the presence of PAH only.

Future work will be devoted to:
Examine the results obtained with several interference filters, with the aim of evidencing PAHs of different molecular weights. Extracting the PAH signal from the combined PAH and soot prompt signal is also possible.
Further study PAH and soot distributions in fuel-rich laminar premixed flames, such as those stabilized at a McKenna burner.
Apply the used techniques to turbulent non premixed flames of interest to the authors (Caetano and Figueira Da Silva, 2015; Cruz and Figueira Da Silva, 2016), in order to investigate the structure of PAH and soot formation, both in the instantaneous and the average senses.

5. ACKNOWLEDGEMENTS

This work has been supported by Petrobras under the technical monitoring of Dr. Ricardo Serfaty (Project: Development of a modeling technique for turbulent combustion based on an Eulerian/Lagrangian approach – Phase II, Contract No.: 0050.0080122.12.9). During this work, Juan José Cruz Villanueva received a PhD scholarship from CNPq (Conselho Nacional de Desenvolvimento Cientifico e Tecnológico) and Luís Fernando Figueira da Silva was on leave from the Institut Pprime (Centre National de la Recherche Scientifique, France).

6. REFERENCES

Axelsson, B., Collin, R. and Bengtsson, E., 2001. "Laser-induced incandescence for soot particle size and volume fraction". *Applied Physics B*, Vol. 72, p. 367-372.

Bejaoui, S., Mercier, X., Desgroux, P. and Therssen, E., 2014. "Laser induced fluorescence spectroscopy of aromatic species produced in atmospheric sooting flames using UV and visible excitation wavelengths". *Combustion and Flame*, Vol. 161, p. 2479-2491

Bladh, H., Johnsson, J. A. and Bengtsson, P. E., 2009. "Influence of spatial laser energy distribution on evaluated soot particle sizes using two-color laser-induced incandescence in a flat premixed ethylene/air flame". *Applied Physics B*, Vol. 96, p. 645-656.

Bladh, H. et al., 2011. "Optical soot characterization using two-color laser-induced incandescence (2C-LII) in the soot growth region of a premixed flat flame". *Proceedings of the Combustion Institute*, Vol. 33, p. 641-648.

Borshanpour, B., 2013. *Development and validation of an experimental apparatus for the characterization of soot in a Laminar Co-Flow Diffusion Flame Using laser-induced incandescence*. Ph.D. thesis, University of Toronto. Toronto.

Bouvier, Y. et al., 2007. "Molecular species adsorbed on soot particles issued from low sooting methane and acetylene laminar flames: A laser-based experiment". *Proceedings of the Combustion Institute*, Vol. 31, p. 841-849.

Caetano, N. R. and Figueira da Silva, L. F., 2015. "A comparative experimental study of turbulent non premixed flames stabilized by a bluff-body burner". *Experimental Thermal and Fluid Science*, Vol. 63, p. 20-33.

Cignoli, F., Benecchi, S. and Zizak, G., 1992. "Simultaneous one-dimensional visualization of OH, polycyclic aromatic hydrocarbons, and soot in a laminar diffusion flame". *Optics Letters*, Vol. 17, p. 229-231.

Cruz, J. J. and Figueira da Silva, L. F., 2016. "Study of the turbulent velocity field in the near wake of a bluff body". *Flow, Turbulence and Combustion*, Vol. 96, p. 1-14.

Dasch, C. J., 1992. "One-dimensional tomography: a comparison of Abel, onion-peeling, and filtered backprojection methods". *Applied Optics*, Vol. 31, p. 1146-1152.

Daun, K. J., Thomson, K. A., Liu, F. and Smallwood, G. J., 2006. "Deconvolution of axisymmetric flame properties using Tikhonov regularization". *Applied Optics*, Vol. 45, p. 4638-4646.

De Luliis, D., Maffi, S., Cignoli, F. and Zizak, G., 2011. "Three-angle scattering/extinction versus TEM measurements on soot in premixed ethylene/air flame". *Applied Physics B*, Vol. 102, p. 891-903.

Desgroux, P., Mercier, X. and Thomson, K. A., 2013. "Study of the formation of soot and its precursors in flames using optical diagnostics". *Proceedings of the Combustion Institute*, Vol. 34, p. 1713-1738.

Escudero, F. et al., 2016a. "Unified behavior of soot production and radiative heat transfer in ethylene, propane and butane axisymmetric laminar diffusion flames at different oxygen indices". *Fuel*, Vol. 183, p. 668-679.

Escudero, F. et al., 2016b. "Effects of oxygen index on soot production and temperature in an ethylene inverse diffusion flame". *Experimental Thermal and Fluid Science*, Vol. 73, p. 101-108.

Fetzer, J., 2007. "The chemistry and analysis of the large PAHs". *Polycyclic Aromatic Hydrocarbons*, Vol. 27, p. 143-162.

Frenklach, M., 2002. "Reaction mechanism of soot formation in flames". *Physical Chemistry Chemical Physics*, Vol. 4, p. 2028-2037.

Gülder, Ö. L., Snelling, D. R. and Sawchuk, R. A., 1996. "Influence of hydrogen addition to fuel on temperature field and soot formation in diffusion flames". *Twenty-Sixth Symposium (International) on Combustion*, Vol. 26, p. 2351-2358.

Hadef, R. et al., 2013. "The concept of 2D gated imaging for particle sizing in a laminar diffusion flame". *Applied Physics B*, Vol. 112, p. 395-408.

Henríquez, R. et al., 2014. "The oxygen index on soot production in propane diffusion flames". *Combustion Science and Technology*, Vol. 186, p. 504-517.

Jenkins, T. P. and Hanson, R., 2001. "Soot pyrometry using modulated absorption/emission". *Combustion and Flame*, Vol. 126, p. 1669-1679.

Legros, G. et al., 2015. "Simultaneous soot temperature and volume fraction measurements in axis-symmetric flames by a two-dimensional modulated absorption/emission technique". *Combustion and Flame*, Vol. 162, p. 2705-2719.

Liu, F., Thomson, K. A. and Smallwood, G. J., 2013. "Soot temperature and volume fraction retrieval from spectrally resolved flame emission measurement in laminar axisymmetric coflow diffusion flames: Effect of self-absorption". *Combustion and Flame*, Vol. 160, p. 1693-1705.

Liu, L. H. and Jiang, J., 2001. "Inverse radiation problem for reconstruction of temperature profile in axisymmetric free flames". *Journal of Quantitative Spectroscopy and Radiative Transfer*, Vol. 70, p. 207-215.

Luch, A., 2005. *The carcinogenic effects of polycyclic aromatic hydrocarbons*. Imperial College Press, London, 1st edition.

Modest, M. F., 2013. *Radiative Heat Transfer*. Academic Press, Oxford, 3rd edition.

Schoemaecker Moreau, C. et al., 2004. "Two-color laser-induced incandescence and cavity ring-down spectroscopy for sensitive and quantitative imaging of soot and PAHs in flames". *Applied Physics B*, Vol. 78, p. 485-492.

Schulz, C. et al., 2006. "Laser-induced incandescence: recent trends and current questions". *Applied Physics B*, Vol. 83, p. 333-354.

Snelling, D. R., Thomson, K. A., Smallwood, G. J. & Gülder, Ö. L., 1999. "Two-dimensional imaging of soot volume fraction in laminar diffusion flames". *Applied Optics*, Vol. 38, p. 2478-2485.

Snelling, D. R. et al., 2002. "Spectrally resolved measurement of flame radiation to determine soot temperature and concentration". *AIAA Journal*, Vol. 40(9), p. 1789-1795.

Vander Wal, R. L., 1996. "Soot precursor material: Visualization via simultaneous LIF-LII and characterization via TEM". *Twenty-Sixh Symposium (International) on Combustion*, Vol. 27(2), p. 2269-2275.

Vander Wal, R. L., 1998. "Soot precursor carbonization: Visualization using LIF and LII and comparison using bright and dark field TEM". *Combustion and Flame*, Vol. 112, p. 607-616.

Vander Wal, R. L., Jensen, K. A. and Choi, M. Y., 1997. "Simultaneous laser-induced emission of soot and polycyclic aromatic hydrocarbons within a gas-jet diffusion flame". *Combustion and Flame*, Vol. 109, p. 399-414.

Xiao, J., Austin, E. and WL, R., 2005. "Relative polycyclic aromatic hydrocarbon concentrations in unsteady counterflow diffusion flames". *Combustion Science and Technology*, Vol. 177, p. 691-713.

Zhao, H. and Ladommatos, N., 1998. "Optical diagnostics for soot and temperature measurement in diesel engines". *Progress in Energy and Combustion Science*, Vol. 24, p. 221-255.

7. RESPONSIBILITY NOTICE

The authors are the only responsible for the printed material included in this paper.